

# Examination of voids and geometry of bio-based braided composite structures

Garrett W. Melenka<sup>1\*</sup>, Brianna M. Bruni-Bossio<sup>2</sup>, Cagri Ayranci<sup>2</sup>, Jason P. Carey<sup>2</sup>

<sup>1</sup> Lassonde School of Engineering, York University, 4700 Keele St. North York, ON M3J 1P3

<sup>2</sup> Mechanical Engineering, University of Alberta, Donadeo Innovation Centre for Engineering, 9211-116 Street NW, Edmonton AB Canada T6G 1H9

\* gmelenka@yorku.ca

**Abstract.** Braided composites are formed by interlacing continuous fibers into a textile pre-form and then impregnating the pre-form within a matrix material. Braid mechanical properties are manipulated through the selection of matrix, fiber and braid geometry. Braided composites are produced with conventional materials like carbon, aramid and glass fibers; however, they can also be produced using natural fibers such as jute, hemp, flax or regenerated cellulose. The mechanical properties of conventional and natural braided composites are highly affected by voids within the braided structure. The effect of voids on braided structures must be investigated to improve braided composite performance. A high-resolution micro-computed tomography ( $\mu$ CT) measurement method was utilized to quantify the size and distribution of voids within natural fiber- bio resin braided composite structures. Image processing techniques were employed to quantify void, matrix and fiber content within 35° and 45° braid samples. Accurate quantification of fiber, matrix and void volumes are crucial for evaluating the quality and repeatability of the braided composite manufacturing process. Reduction of voids and pores will improve braided composite mechanical properties and performance. Measurement of the constituents within braided composites is also necessary for the development of accurate models for predicting braid mechanical properties. Measurement of the internal microstructure of braided composites will allow for the development of improved analytical and numerical braided composite models.

## 1. Introduction

Braided composites are an advanced textile-based manufacturing process that create near-net-shape structures by interlacing continuous fiber yarns into a pre-form [1], [2]. Two dimensional (2D) tubular braids are commonly formed using a Maypole braiding machine while three dimensional (3D) braids are formed using Cartesian or rotatry braiding machines [3]. Braided composites are produced by impregnating (or wetting) the braided pre-form with a matrix material.

Presently, braided composites have been manufacturing using conventional composite fibers including carbon, aramid and glass fibers. The braid manufacturing technique can also be adapted to bio-based fibers such as hemp, jute, flax or cellulose [4]–[7]. Additionally, bio-based resins and polymers can also be used as the matrix material for braided structures [4], [8]. The ability to use a wide range of matrix and fiber materials demonstrates the versatility of the braided composite manufacturing process. Bio-based composites are an example of an emerging alternative to conventional composites that can be produced sustainably while yielding comparable mechanical properties [9]–[11].



Accurate measurement and analysis of braided composite structures is required so that these products can be used for structural applications and other strategically critical applications. Analytical and numerical models require data such as braid angle ( $\theta$ ), yarn width ( $W_y$ ), yarn thickness ( $t$ ), matrix volume fraction ( $v_m$ ), fiber volume fraction ( $v_f$ ) and void volume fraction ( $v_v$ ) to accurately predict braid mechanical properties [12]–[15]. Geometric data of braided structures can be obtained using methods such as optical microscopy or scanning electron microscopy (SEM) however, these methods are limited to two dimensional (2D) cross-sections for analysis [16]. Optical microscopy and SEM measurements are also destructive measurement methods. The internal geometry of composite structures can be evaluated using an X-ray based micro-computed tomography ( $\mu$ CT) technique [17]–[19]. This approach allows for the non-destructive analysis of voids throughout the composite material micro-structure [20]. The  $\mu$ CT has advantages over conventional measurement methods since the three dimensional (3D) geometry of a sample can be analyzed. Braided and woven composite structures have complex 3D geometries and the  $\mu$ CT measurement method allows for the visualization and evaluation of these structures [16], [17], [21]. Additionally, the  $\mu$ CT measurement method allows for the quantification of voids and defects within composite structures [18], [20], [22]. The  $\mu$ CT method is advantageous over conventional resin burn off or acid digestion methods since the size and distribution of voids within braided structures can be obtained.

The study by Melenka *et al.* [22] examined the geometry and void content of a tubular braided composite manufactured using conventional aramid yarns within an epoxy matrix. A Diamond (1/1) braided geometry was examined and a single braiding angle was considered. The braid sample was examined using a voxel size of  $18.2 \mu\text{m}^3$  allowing for the entire braid cross-section to be examined however, details analysis of individual fiber tows was not possible. Additionally, the yarn size and shape of 3D braided composites was also examined by Ya *et al.* [18]. A resolution of  $10 \mu\text{m}^3$  was achieved in the study by Ya *et al.* The studies that have examined braided structures using the  $\mu$ CT method have focused on the overall braid geometry. A detailed investigation of a braid unit cell has not been performed using this measurement approach.

Voids and open pores that occur within braided composite structures will produce failure initiation sites within the braided composite structure and therefore have a negative impact on mechanical properties [20], [23], [24]. Using the  $\mu$ CT measurement method the size and distribution of voids within natural fiber- bio resin braided composite structures will be examined. The effect of braiding angle on the voids size and distribution will also be investigated. Resin, fiber and void volume fractions will be quantified using the  $\mu$ CT measurement method. Accurate quantification of fiber, matrix and void volumes are crucial for evaluating the quality and repeatability of the braided composite manufacturing process. Reduction of voids and pores will improve braided composite mechanical properties and performance. Measurement of the constituents within braided composites is also necessary for the development of accurate models for predicting braid mechanical properties.

## 2. Methods

2D tubular braided tubular composite samples were manufactured using a Maypole braiding machine (Steege USA, K80–72, Steeger USA, Inman, SC). The samples were manufactured in a full-load configuration consisting of 36 yarn carriers resulting in a Regular (2/2) braid pattern [2]. Samples were produced with two different braiding angles ( $35^\circ$  and  $45^\circ$ ). Regenerated cellulose fibers (BioMid™, 1650 Denier, ENC International Inc, Burnaby, BC, Canada) formed the braided preform. After the braid performs were manufactured, the samples were placed onto 9.525mm (3/8") polytetrafluoroethylene (PTFE) mandrels and impregnated with a bio-based resin (SuperSap One, Entropy Resins, Bay City, MI). Each sample was cured at room temperature for seven days to reach full cure.

A high resolution micro-computed tomography technique was used to evaluate the geometry and void content of natural fiber/ bio-based resin braided composite structures. Current studies have examined conventional fibers and matrix materials using the  $\mu$ CT measurement method [18], [22]. The braid samples were evaluated using a SkyScan 1272 microtomograph (Bruker-MicroCT, Kontich, Belgium). Images of the braid samples were collected at a resolution of 4904x3280 pixels. The settings

for the  $\mu$ CT scan of each braid sample are detailed in Table 1. The settings shown in Table 1 were selected to optimize contrast between the matrix and fiber materials. The scan time for each of the braid samples using the listed settings was approximately 60 minutes. The final image voxel size for each sample was set at  $1.0\ \mu\text{m}^3$  to achieve sufficient resolution to observe voids and individual fiber filaments within the braided structures.

**Table 1.** Micro-computed tomography ( $\mu$ CT) scan parameters

$\mu$ CT Parameter	Value
X-Ray Voltage	40 kV
Current	200 $\mu\text{A}$
Frame Averaging	2
Rotation Step	$0.2^\circ$
Number of Projections	900
Projection Exposure Time	1316 ms
Detector Pixel Size	$7.4\ \mu\text{m}$
Reconstructed Image Pixel Size	$1.0\ \mu\text{m}$

A schematic of the tubular braid sample and sample mount are shown in Figure 2. The custom sample holder was designed using a computer aided design package (SolidWorks 2018, Dassault Systems, France). The sample mount was manufacturing using a 3D printer (Select Mini V2, MonoPrice, Brea, CA). As shown in Figure 2, the sample mount offset the centerline of the braided composite samples from the rotation axis of the  $\mu$ CT machine by 4.0mm. Offsetting the rotation axes of the braided composite sample allowed for a high resolution scan of a segment of each of the braid samples to be examined.

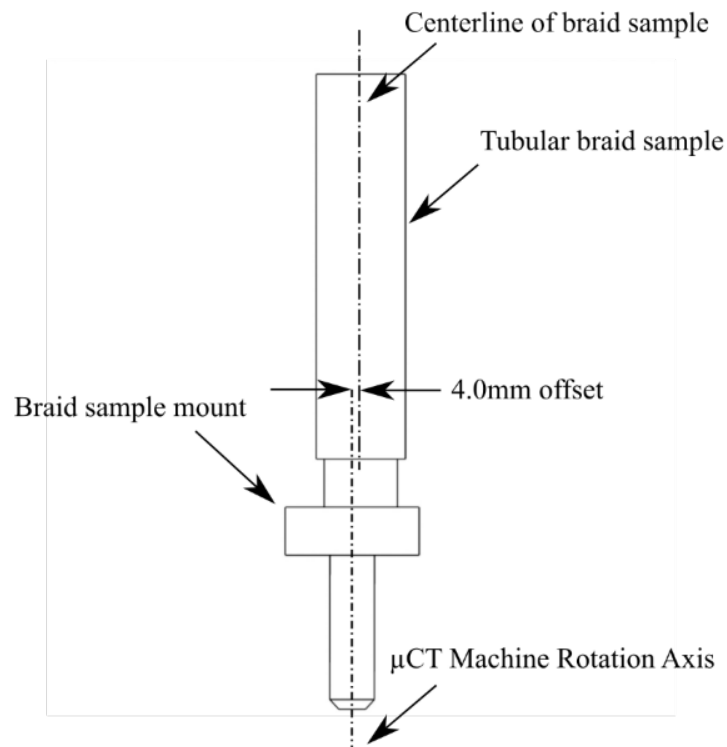


**Figure 1.** Tubular braided composite  $\mu$ CT sample mount

Radiograph images of the braided composite were collected for the two braid sample. Example radiographs of the  $35^\circ$  and  $45^\circ$  braid samples are shown in Figure 2. In this image, the braid samples

can be seen off-set from the center of the radiograph image due to the sample mount shown in Figure 1. Large pores within the braided composite sample can be observed in the radiographs shown in Figure 2. As shown in Table 1, 900 radiographs were obtained for each braid sample. The collected radiographs allowed for a segment of each braid to be reconstructed for detailed analysis. The radiograph images were imported into a reconstruction software (NRECON 1.7.1.0, Bruker, Belgium) to create cross-sectional images of the braided composite as seen in Figure 3. In Figure 3, grayscale contrast indicating the matrix and fibers can be seen in the braid cross-sectional image as well as the varying braid geometry of the 35° and 45° braids. The grayscale variations in Figure 3 enable the quantification of the resin, matrix and void content within each braid sample. All reconstructed cross-sectional images were exported as 8-bit bitmap (BMP) images with an image size of 4904 x 4904 pixels for analysis.

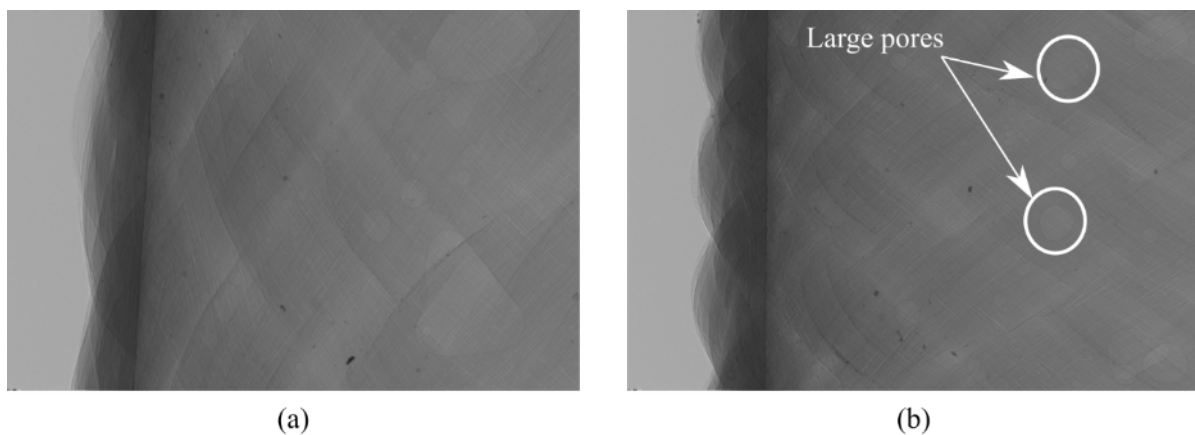


**Figure 2.** Example radiographs of tubular braided composite samples (a) 35° braid (b) 45° braid. Voids, fibers and matrix material can be seen in each of the radiographs

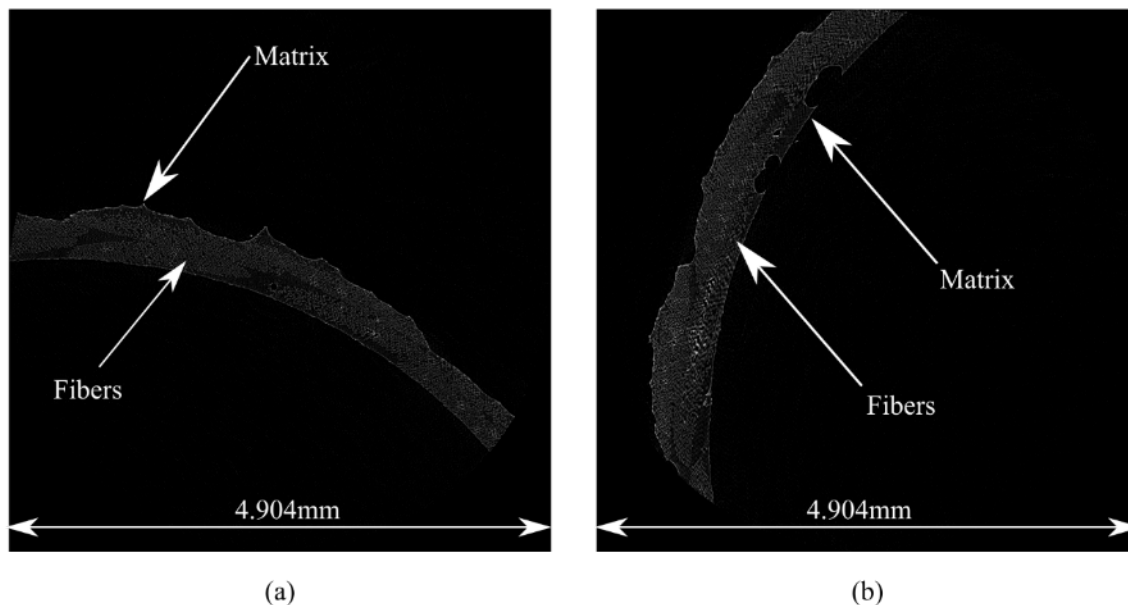


**Figure 3.** Representative reconstructed cross-sectional images of tubular braid samples (a) 35° braid 1.0  $\mu\text{m}$  scan resolution (b) 45° braid 1.0  $\mu\text{m}$  scan resolution. Braid yarn geometry, voids and the reinforcing matrix can be seen with varying grayscale intensity.

### 2.1. Braid Morphology

Image segmentation was performed on the braid sample cross-sectional images to identify braid features [25]. Segmentation of the collected braid cross-sectional images was performed using an image analysis and visualization software package (CTan 1.16.90, Bruker microCT, Belgium). The image segmentation procedure identified matrix, fibers, and voids within the braid structure. The following image segmentation procedure was used to quantify the constituents of the braid sample. To remove noise from the braid cross-section images a Gaussian Blur operation was used with a circular structuring element of 1 pixel. The braid yarns were determined by thresholding the braid sample using a threshold range of 30-120. Similarly, the resin was identified by thresholding the braid sample using a threshold of 10-30. The segmented braid yarns and matrix for both 35° and 45° braid samples are shown in Figure 4. The identified fibers and matrix materials for both braid samples are shown in this figure.

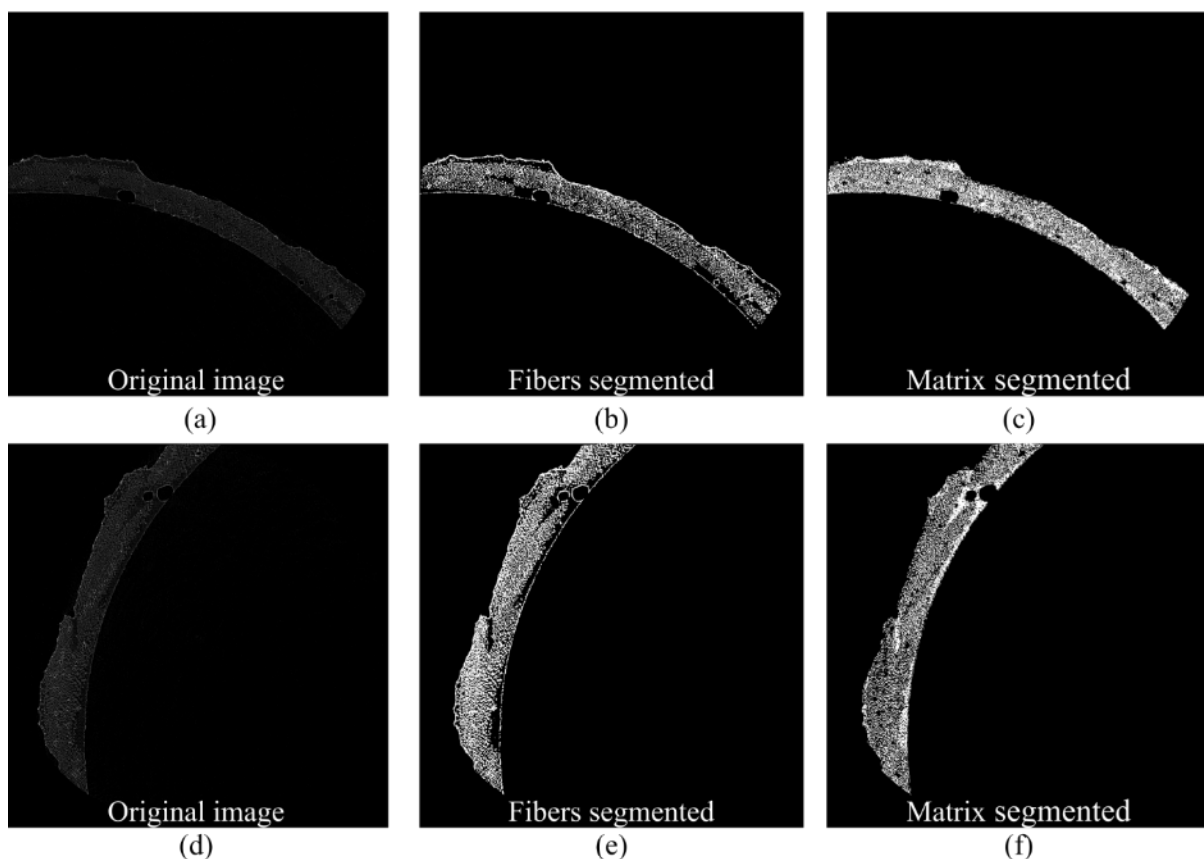


**Figure 4.** Matrix and fiber segmentation (a) 35° original braid cross section (b) 35° braid segmented yarns (c) 35° segmented matrix (d) 45° original cross-section (e) 45° segmented yarns (f) 45° segmented matrix

### 2.2. Yarn Morphology

Individual braid yarns were also examined for both the 35° and 45° braid angle samples. Individual yarns were identified using the region-of-interest “ROI” tool in CTan to identify a single fiber tow from within the braid geometry. An example of idealized braid yarns used in the prediction of the mechanical properties of Diamond and Regular braid are shown in Figure 5 [26]. The identified braid fiber tows can be seen in Figure 6. In Figure 6 (a) and (b) an individual fiber tow is identified for the 35° and 45° braid respectively. The braid tows were segmented to identify individual fibers as shown in Figure 6 (c) and (d). The identified individual fibers with the tow will be compared with the manufacture data to assess the number of fiber filaments within a single tow. Additionally, the geometry of an individual fiber tow

was also identified as shown in Figure 6 (e) and (f). The total cross-sectional area, major diameter, and minor diameter of the fiber tow are calculated from the segmented images shown in Figure 6 (e) and (f) to assess the effect of braiding angle on tow geometry.

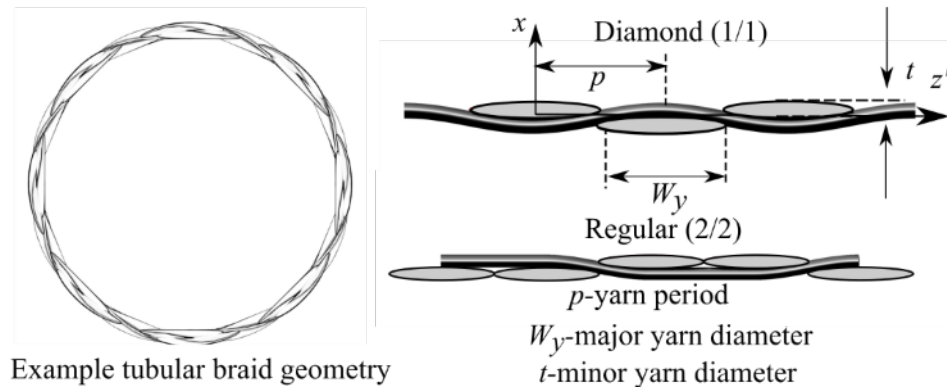


**Figure 5.** Example idealized braid geometries used for predicting mechanical properties

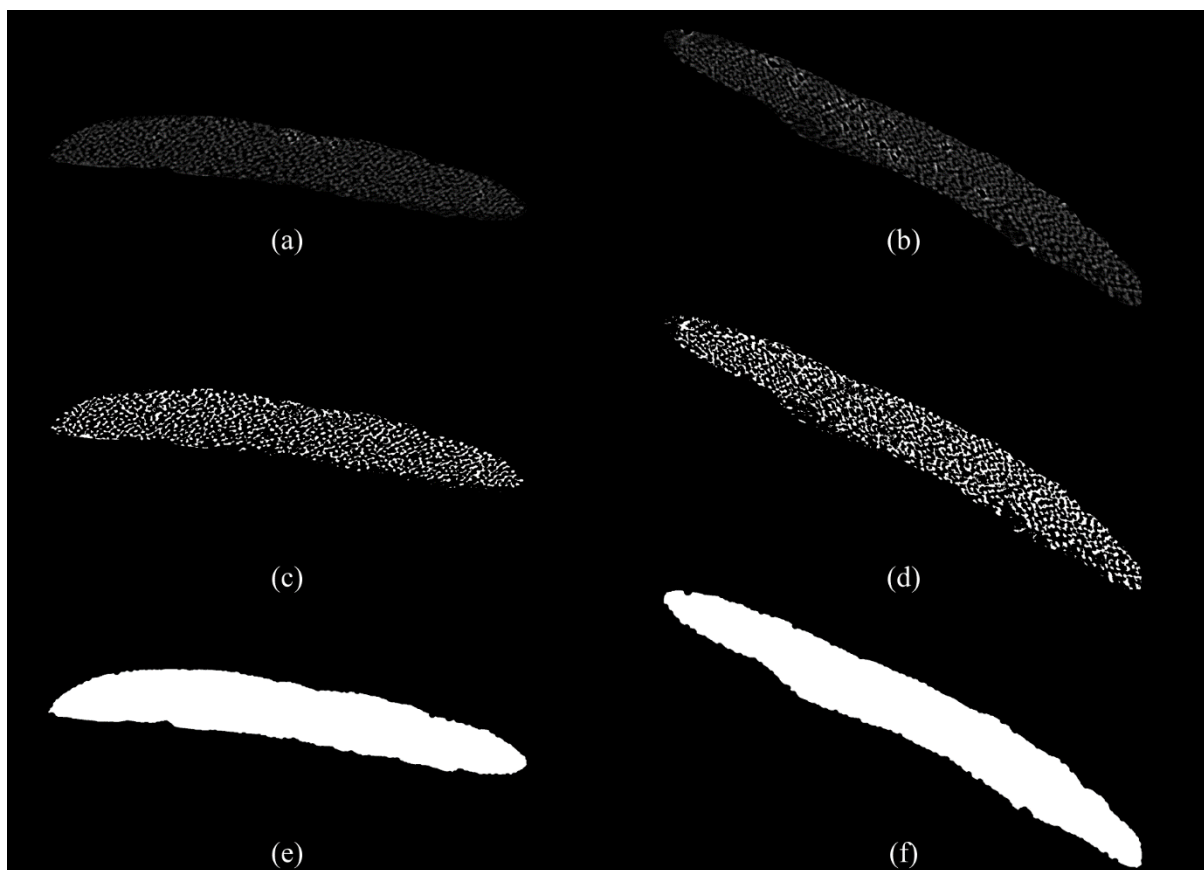


**Figure 6.** Identification of individual braiding yarns (a) 35° braid yarn (b) 45° braid yarn (c) Segmented 35° braid yarn where individual fibers are identified (d) Segmented 45° braiding yarn with identified fibers (e) Identified 35° fiber tow (f) Identified 45° fiber tow.

### 2.3. Braid Void Analysis

Voids and open pores were identified using an image segmentation algorithm. Examples of voids within the braided composite sample cross-section are shown in Figure 7. Enclosed voids are shown in Figure 7 (a) where the enclosed voids occur within the inner and outer diameters of the braid samples. Open pores, shown in Figure 7 (b), occur along the inside and outside diameter of the braid.

The identification process for voids within the braid samples is shown in Figure 8. Voids in the braid samples were identified by using a threshold of 10-120 (Figure 8 (b)). All voids were removed from the segmented image to allow for individual void identification (Figure 8 (c)). Open pores, Figure 8 (d), were identified using the “Shrink-wrap” function in CTan to locate all open pores that exist along the inner and outer braid diameters. Fully enclosed voids, Figure 8 (e), were identified using the “Despeckle-remove pores” function in CTan to identify all fully voids which are fully enclosed within the braid geometry. All enclosed voids and open pores can be seen in Figure 8 (f). The generated binary images shown in Figure 8 allow for the size and distribution of voids and pores to be analyzed throughout the 3D braid geometry. The “Individual Object Analysis” tool in CTan was used to calculate the volume, major diameter, and minor diameter of all voids and pores identified for each braid geometry. After each segmentation, a 3D volume was created using the “Double-Time Cubes” stereolithography (STL) algorithm in CTan. Finally, the 3D fiber, resin and void volumes were visualized using an open-source visualization software (ParaView 5.4.1, Kitware, Clifton Park, NY) to visualize the spatial distribution of the segmented braid features.

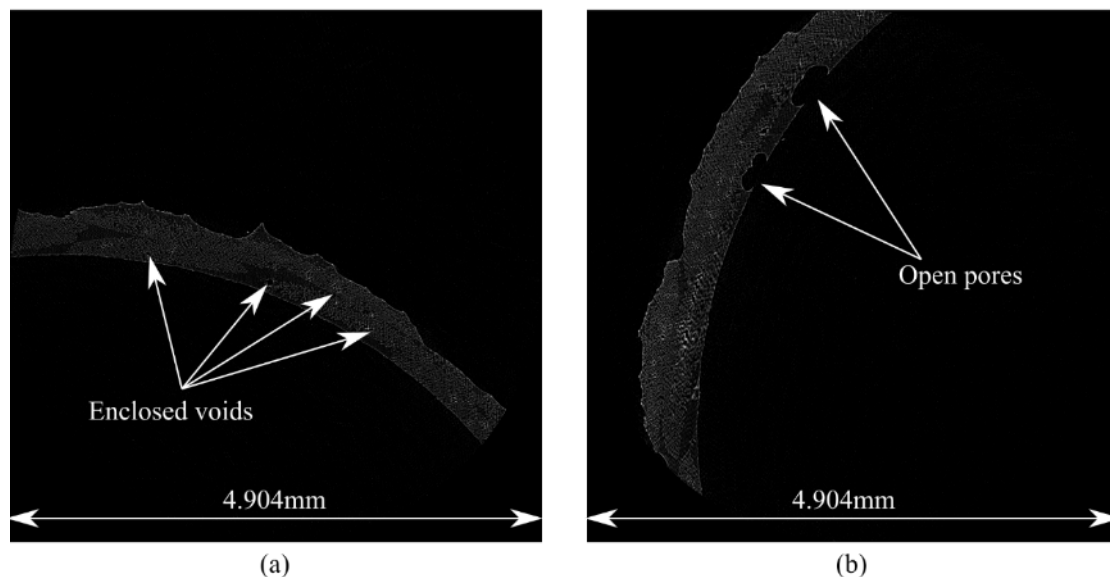


**Figure 7.** Void Examples (a) Enclosed voids (b) Open pores

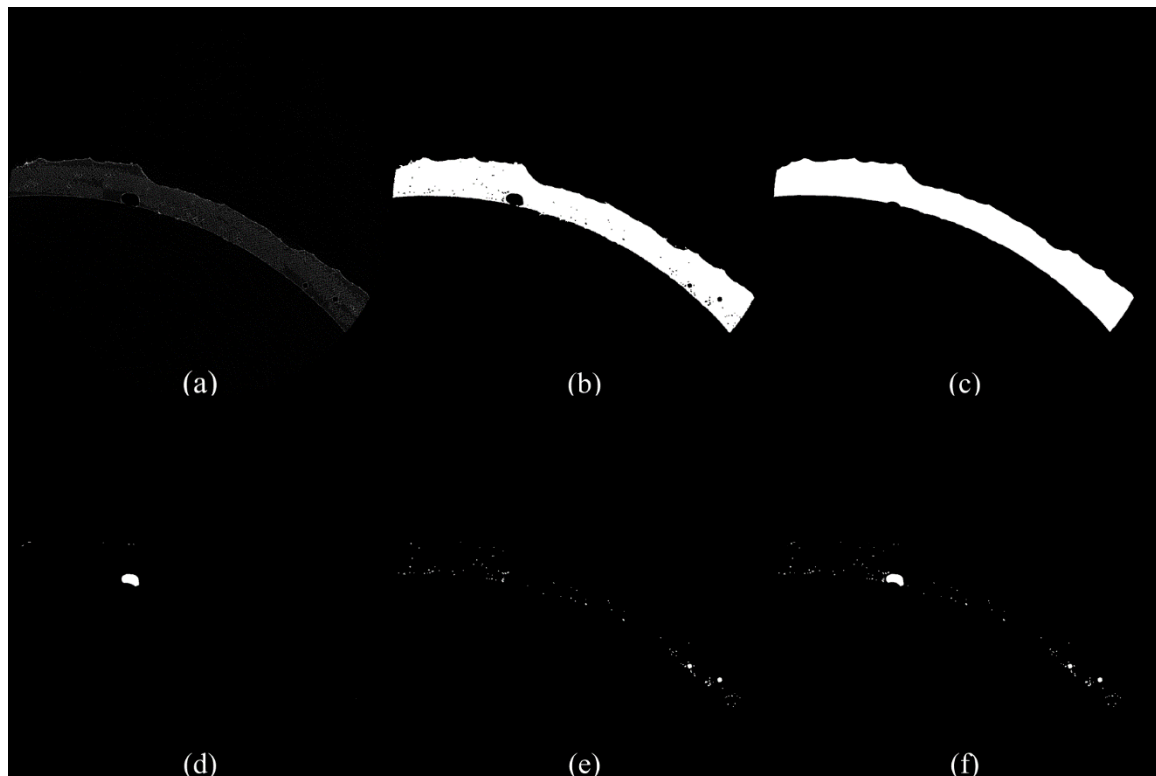


**Figure 8.** Braid void segmentation procedure (a) original braid cross-section, (b) thresholded cross-section showing enclosed voids and open pores, (c) braid geometry with open pores and enclosed voids filled, (d) identified open pores, (e) identified closed voids, (f) identified open pores and closed voids

### 3. Results and Discussion

#### 3.1. Braid Morphology

The resulting 3D geometries for the 35° and 45° braid samples are shown in Figure 9. The open pore and enclosed void distribution is visualized for both braid geometries. In addition, the matrix and fiber distribution for both geometries are shown. The distribution of voids relative to the braid matrix and fiber volumes can also be seen. From Figure 9 it can be seen that enclosed voids commonly occur along the braid yarn paths. A significant portion of enclosed voids occur at the cross-over region between braiding yarns. Also seen in Figure 9 are several large pores which were formed along the inside and outside diameters of the braid. Large spherical pores occur along the inside diameter of the braid while elliptical or elongated pores occur along the outside diameter of each braid. The three dimensional geometries of the two braid samples can also be seen in Figure 9 (g) and (h).

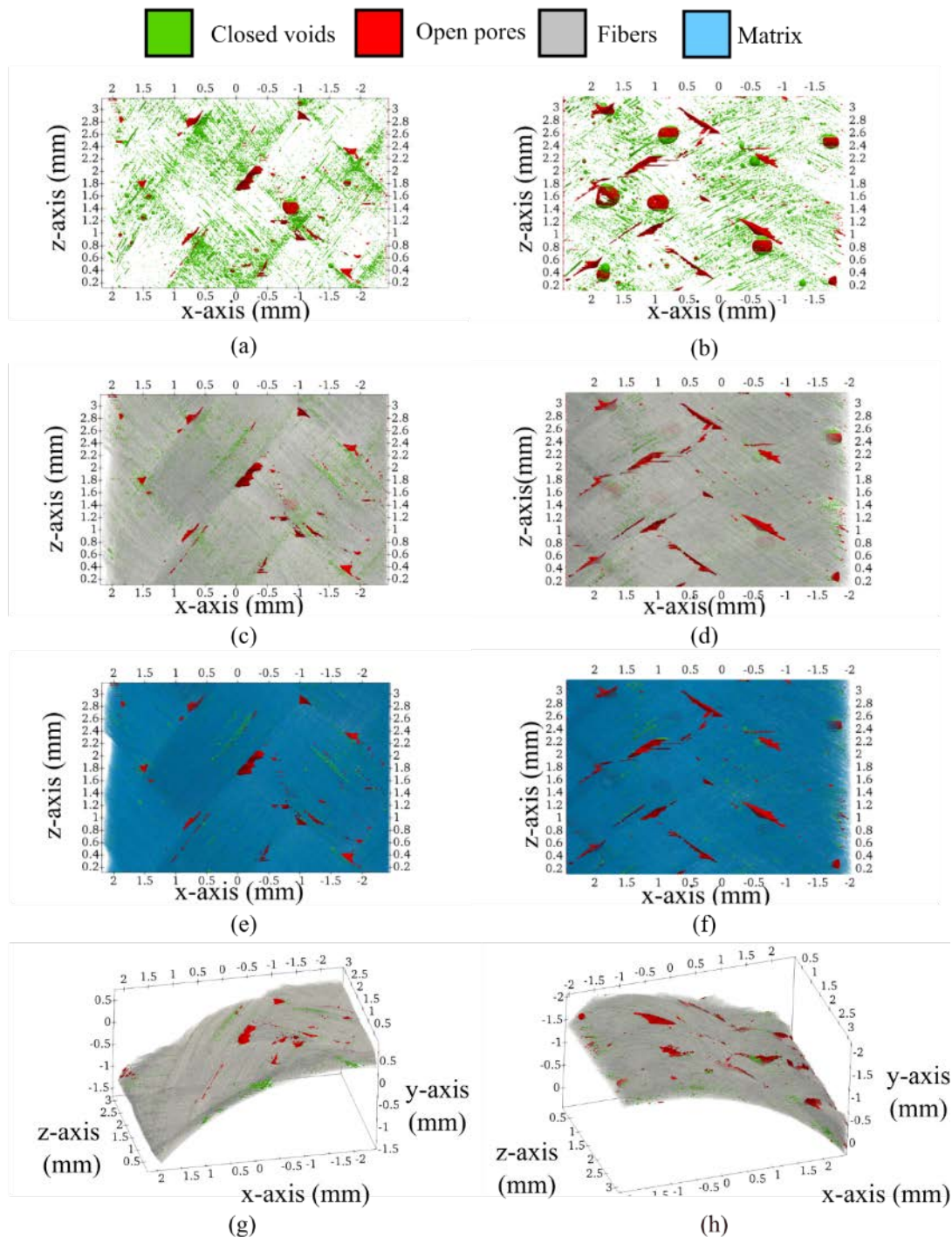


**Figure 9.** 3D visualization of braid geometry (a) 35° braid closed void and open pore distribution (b) 45° braid closed void and open pore distribution (c) 35° braid fiber distribution with voids shown (d) 45° braid fiber distribution with voids shown (e) 35° braid matrix distribution with voids shown (f) 45° braid with voids shown.

The total fiber volume  $V_f$ , matrix volume  $V_m$ , enclosed void volume  $V_{vc}$  and open pore volume  $V_{vo}$  and total void  $V_T$  volumes were calculated for each braid geometry. The calculated volumes for both

braid samples are summarized in Table 2. The fiber volume fraction ( $v_f$ ), matrix volume fraction ( $v_m$ ) and closed void volume fraction ( $v_{vc}$ ) and open pore volume fraction ( $v_{vo}$ ) were calculated using Equations (2) - (5). The total void volume fraction ( $v_T$ ) is the sum of the open pore and closed void volume fractions as shown in Equation (1).

$$v_f = \frac{V_f}{V_f + V_m + V_{vc} + V_{vo}} \quad (2)$$

$$v_m = \frac{V_m}{V_f + V_m + V_{vc} + V_{vo}} \quad (3)$$

$$v_{vc} = \frac{V_{vc}}{V_f + V_m + V_{vc} + V_{vo}} \quad (4)$$

$$v_{vo} = \frac{V_{vo}}{V_f + V_m + V_{vc} + V_{vo}} \quad (5)$$

$$v_T = v_{vc} + v_{vo} \quad (6)$$

Table 2 shows that there is an increase in fiber volume and fiber volume fraction as braiding angle increases. Additionally, the 45° braid sample exhibited a greater number of open pores and total void volume. The increased number of open pores is a result of the increased braiding angle. Braid samples manufactured in this study were not cured under a vacuum and as a result air can become entrapped between the braid mandrel and fibers curing sample curing resulting in the large open pores observed. The matrix volume fraction was also observed to decrease with increasing braiding angle. The lower fiber volume fraction in the 35° results in an increase in the matrix volume fraction within the braid geometry. As fiber volume fraction increases, matrix volume fraction will decrease due to fiber compaction within the braid structure.

**Table 2.** Braid calculated fiber, matrix and void volumes

Sample	35° braid	45° braid
Fiber Volume $V_f$ (mm <sup>3</sup> )	2.0939	3.5266
Matrix Volume $V_m$ (mm <sup>3</sup> )	3.9081	3.3608
Closed Void Volume $V_{vc}$ (mm <sup>3</sup> )	0.0660	0.0663
Open Pore Volume $V_{vo}$ (mm <sup>3</sup> )	0.0153	0.0615
Total Void Volume (mm <sup>3</sup> )	0.0812	0.1278
Total Volume (mm <sup>3</sup> )	6.0832	7.0152
Fiber Volume Fraction $v_f$	34.42%	50.27%
Matrix Volume Fraction $v_m$	64.24%	47.91%
Closed Void Volume Fraction $v_{vc}$	1.08%	0.94%
Open Pore Volume Fraction $v_{vo}$	0.25%	0.88%
Total Void Volume Fraction $v_T$	1.34%	1.82%

### 3.2. Yarn Morphology

Individual fiber tows for the 35° and 45° braids were examined to determine the total fiber tow cross-sectional area and to determine the fiber tow major and minor diameters. The measured fiber tow area, major diameter and minor diameter for selected braid yarns are summarized in Table 3. The measured

tow major diameter and minor diameter correspond to the yarn width ( $W_y$ ) and thickness ( $t$ ) measurements utilized by authors to describe braid yarn geometry for analytical and numerical modelling [26]–[28]. Accurate measurement of fiber tow dimensions is critical for accurate model development for tubular braided composites. Table 3 demonstrates that the fiber tow major, minor diameters and cross-sectional area vary with braiding angle. As seen in Table 3 the yarn major diameter increases within braiding angle. The increase in yarn major width or major diameter is a result on the increased fiber compaction that occurs with an increasing braid angle. The differences in yarn major and minor diameters can be observed in the yarn images shown in Figure 6. The geometry of braid yarns was also examined by Melenka *et al.* [22]. A single braid with a Diamond braiding pattern was examined. Accurate measurement of the effect of braiding angle on yarn dimensions is critical for the accurate prediction of braid mechanical properties.

**Table 3.** Braid fiber tow analysis

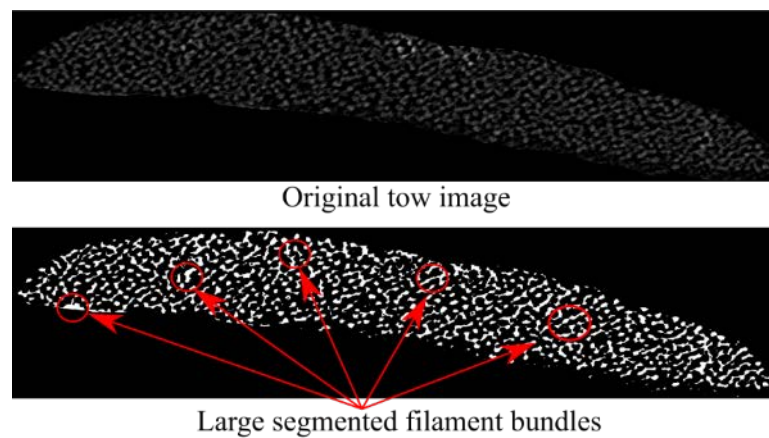
Sample	35° braid	45° braid
Fiber Tow Area (mm <sup>2</sup> )	0.2928±0.0032	0.4043±0.0287
Fiber Tow Major Diameter (mm)	1.6946±0.0036	2.1189±0.0594
Fiber Tow Minor Diameter (mm)	0.2177±0.0038	0.2584±0.0217

Individual braid tows were also examined to identify the individual fiber filaments within a fiber tow. The identified filaments within a fiber tow can be seen in Figure 6 (c) and (d). The results from the braid tow analysis is shown in Table 4. The total number of identified filaments are summarized as well as the total filament area and average major and minor diameters of each of the individual filaments.

**Table 4.** Braid yarn filament analysis

Sample	35° braid	45° braid
Number of Filaments Identified	685±25	673±60
Filament Area (μm <sup>2</sup> )	96.67±5.20	169.40±10.33
Filament Major Diameter (μm)	16.87±0.58	20.49±0.99
Filament Minor Diameter (μm)	7.64±0.27	9.52±0.49

The cellulose yarns that were used in this study have a fiber denier of 1650 and are reported to consist of 900 filaments with a filament diameter of 11μm. From Table 4 it can be seen that 685±25 and 673±60 filaments were identified for the 35° and 45° fiber tows respectively. The measured number of fiber filaments was lower than the manufacturer specifications. The lower number of identified filaments within the fiber tow is most likely due to the image segmentation process. The proximity of the fiber filaments to one another can result in an underestimate of the total number of filaments within the fiber tow. Figure 10 shows a number of large objects that were identified from the image segmentation process. The presence of these large objects results in an underestimate of the true number of filaments within the braid tow. Improvement to the image segmentation algorithm and contrast within the fiber tow images will allow for better identification of individual filaments within the braid tow. The average major diameter of the tow filaments was found to be 16.86±0.57 and 20.48±0.98 μm for the 35° and 45° braids respectively. The measurements of the filament diameter also suggest that all individual yarns have not be identified as the reported diameter of the cellulose filaments is 11μm. The segmentation and analysis of individual filaments within the braid yarns could be improved by the addition of a contrast enhancement agents such as zinc iodide to aide in filament segmentation [16]. A higher resolution μCT scan with a resolution of less than 1.0μm may also be required to identify all tow filaments. Finally, the SkyScan 1272 μCT utilized in this study is capable of achieving a scan resolution of 0.25μm which will allow for improved resolution of individual fiber filaments.

**Figure 10.** Fiber filament identification

### 3.3. Braid Void Analysis

The void distribution throughout both the 35° and 45° samples was examined to quantify the range of open pore and closed void size throughout both samples. The identified closed voids and open pores for both braiding samples are shown in Figure 11. Figure 11 demonstrates that there are significantly more closed voids within both the 35° and 45° braid samples than open pores. Measurement of the average closed void and open pore volumes are also summarized in Table 5. Figure 11 (a) and (b) show that a total of 2204 and 1862 closed voids were identified for the 35° and 45° braids respectively. Similarly, Figure 11 (c) and (d) shows that a total of 119 and 148 open pores were identified for the 35° and 45° braid samples. The void distribution is visualized for both braid geometries in Figure 9. This figure also demonstrates that there are a significantly more closed voids within both braid geometries than open pores.

The average open pore and closed pore volumes and maximum closed void and open pore volumes are summarized in Table 5. Table 5 demonstrates that the open pore volumes found within the two braid samples are an order of magnitude greater than the fully enclosed voids in both samples. The presence of open pores can be significantly minimized by utilizing a vacuum assisted resin transfer molding procedure (VARTM) to ensure improved permeation of the matrix material throughout the braided composite structures. A VARTM process would also assist in decreasing the quantity of closed voids that occur within the braided structure.

**Table 5.** Average closed void and open void volumes

Sample	35° braid	45° braid
Closed Void Average Volume (mm <sup>3</sup> )	1.90E-05	2.50E-05
Maximum Closed Void Volume (mm <sup>3</sup> )	7.40E-04	2.40E-03
Number of Identified Closed Voids	2204	1862
Open Pore Average Volume (mm <sup>3</sup> )	1.23E-04	4.11E-04
Maximum Open Pore Volume (mm <sup>3</sup> )	5.02E-03	9.00E-03
Number of Identified Open Pores	119	148

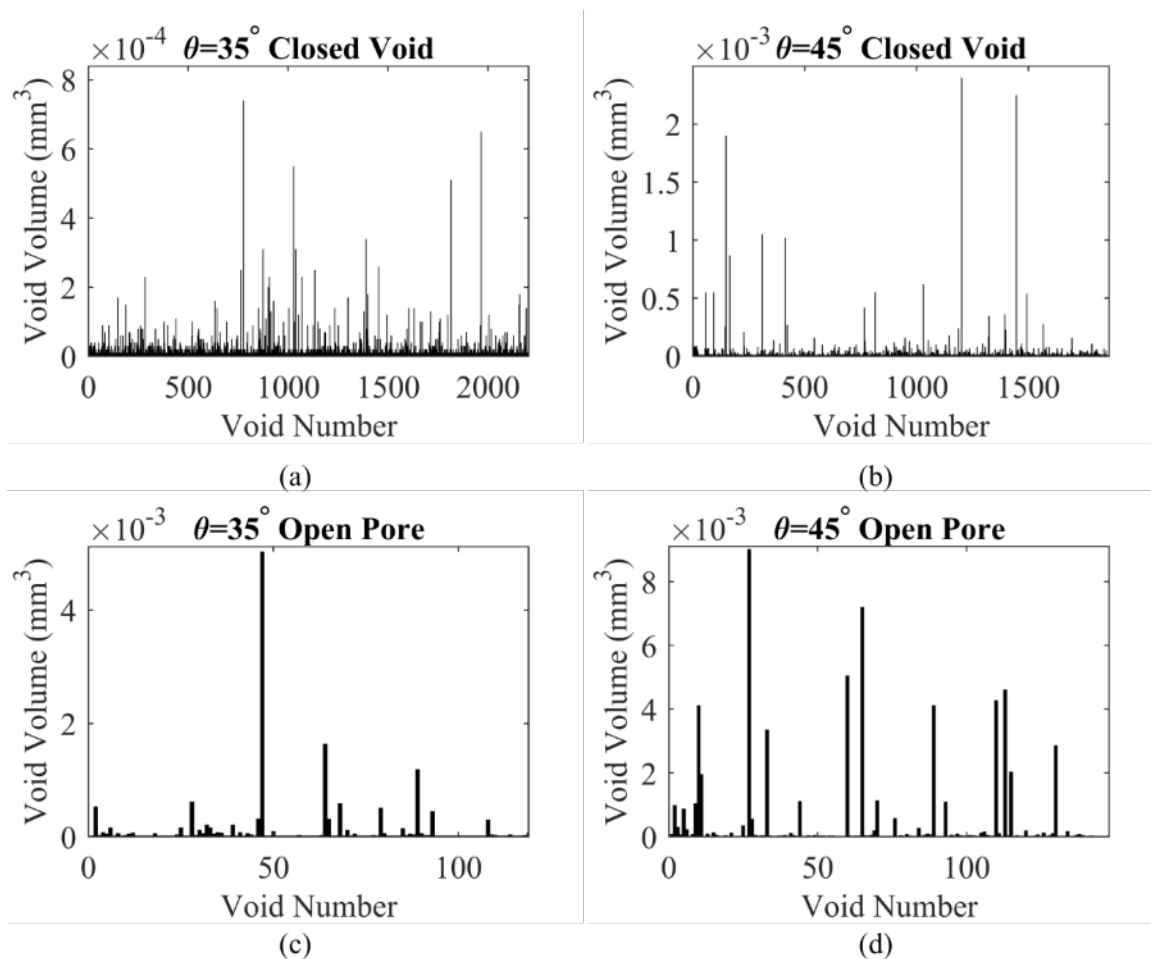


**Figure 11.** Identified closed void and open pores (a) 35° braid closed voids (b) 45° braid closed voids (c) 35° open pores (d) 45° open pores

#### 4. Conclusions

Braided composite samples were examined using a high resolution  $\mu$ CT measurement technique to quantify the sample void, matrix and fiber contents. The braids used in this study were manufactured with braiding angles of 35° and 45° and were produced using natural cellulose fibers and a bio-based resin. The braid samples were scanned using a  $1.0\mu\text{m}^3$  voxel size to examine the microstructure of each braid sample. Two braiding angles were selected to allow for the effect of braid angle on geometry to be investigated. In addition, the void distribution throughout each sample was also examined. The total void volume fraction for the 35° and 45° braids was determined to be 1.34 and 1.82% respectively.

Individual fiber tows were also investigated for the manufactured 35° and 45° braid samples. The overall tow geometry was examined for the two manufactured braid geometries to demonstrate the effect of braid angle on fiber tow geometry. The major diameters for the 35° and 45° samples was measure to be 1.6946 and 2.1189 mm respectively. The results from the fiber tow measurement demonstrate the change in fiber tow geometry with braiding angle. Accurate measurement of fiber tow geometry is required to support analytical and numerical models for braided composite structures.

Finally, individual filaments were examined for fiber tows within each of the braid geometries. Individual fiber filaments were identified however the results from the filament analysis indicate that a higher resolution  $\mu$ CT scan or improve image segmentation process will be required for improved analysis of fiber filaments within braided structures.

This study demonstrates that the  $\mu$ CT measurement technique is a highly effective measurement tool for assessing the geometry of braided composite structures. Open pores and closed voids were identified for two braid samples and their distribution throughout both samples was examined. The overall matrix and fiber content for both samples was also quantified. Individual fiber tows were also examined. The method demonstrated in this work will allow for assessing the manufacturing consistency of braided composite structures. Geometric measurements will also support analytical and numerical models used to predict braided composite mechanical properties.

### Acknowledgments

The authors acknowledge the funding support from the Natural Sciences and Research Council (NSERC) Canada and for support from the Department of Mechanical Engineering of the Lassonde School of Engineering.

### References

- [1] D. Brunnschweiler, "Braids and Braiding," *J. Text. Inst. Proc.*, vol. 44, no. 9, pp. P666–P686, 1953.
- [2] G. W. Melenka *et al.*, "Manufacturing processes for braided composite materials," in *Handbook of Advances in Braided Composite Materials: Theory, Production, Testing and Applications*, 2016, pp. 47–153.
- [3] F. K. Ko, "Braiding," vol. 21, pp. 69–77, 2001.
- [4] S. Kobayashi and K. Takada, "Processing of unidirectional hemp fiber reinforced composites with micro-braiding technique," *Compos. Part A Appl. Sci. Manuf.*, vol. 46, no. 1, pp. 173–179, 2013.
- [5] S. Kobayashi, K. Takada, and D. Song, "Effect of Molding Condition on the Mechanical Properties of Bamboo- Rayon Continuous Fiber / Poly ( Lactic Acid ) Composites," *Adv. Compos. Mater.*, vol. 21, no. 1, pp. 79–90, 2012.
- [6] A. Memon and A. Nakai, "The Processing Design of Jute Spun Yarn / PLA Braided Composite by Pultrusion Molding," *Adv. Mech. Eng.*, vol. 2013, pp. 1–8, 2013.
- [7] I. I. Qamhia, S. S. Shams, and R. F. El-Hajjar, "Quasi-Isotropic Triaxially Braided Cellulose-Reinforced Composites," *Mech. Adv. Mater. Struct.*, vol. 22, no. 12, pp. 988–995, 2015.
- [8] J. Datta and M. Włoch, "Selected biotrends in development of epoxy resins and their composites," *Polym. Bull.*, vol. 71, no. 11, pp. 3035–3049, 2014.
- [9] P. Wambua, J. Ivens, and I. Verpoest, "Natural fibres: Can they replace glass in fibre reinforced plastics?," *Compos. Sci. Technol.*, vol. 63, no. 9, pp. 1259–1264, 2003.
- [10] R. Dunne, D. Desai, R. Sadiku, and J. Jayaramudu, "A review of natural fibres, their sustainability and automotive applications," *J. Reinf. Plast. Compos.*, vol. 35, no. 13, pp. 1041–1050, 2016.
- [11] F. P. La Mantia and M. Morreale, "Green composites: A brief review," *Compos. Part A Appl. Sci. Manuf.*, vol. 42, no. 6, pp. 579–588, 2011.
- [12] J.-H. Byun, "The analytical characterization of 2-D braided textile composites," *Compos. Sci. Technol.*, vol. 60, no. 5, pp. 705–716, Apr. 2000.
- [13] S. C. Quek, A. M. Waas, K. W. Shahwan, and V. Agaram, "Analysis of 2D triaxial flat braided textile composites," *Int. J. Mech. Sci.*, vol. 45, no. 6–7, pp. 1077–1096, 2003.
- [14] M. M. Shokrieh and M. S. Mazloomi, "An analytical method for calculating stiffness of two-dimensional tri-axial braided composites," *Compos. Struct.*, vol. 92, no. 12, pp. 2901–2905, Nov. 2010.
- [15] L. Xu, S. J. Kim, C. H. Ong, and S. K. Ha, "Prediction of material properties of biaxial and triaxial braided textile composites," *J. Compos. Mater.*, vol. 46, no. 18, pp. 2255–2270, 2012.
- [16] L. P. Djukic, I. Herszberg, W. R. Walsh, G. a. Schoepner, B. Gangadhara Prusty, and D. W. Kelly, "Contrast enhancement in visualisation of woven composite tow architecture using a MicroCT Scanner. Part 1: Fabric coating and resin additives," *Compos. Part A Appl. Sci.*

- Manuf.*, vol. 40, no. 5, pp. 553–565, May 2009.
- [17] R. G. Rinaldi, M. Blacklock, H. Bale, M. R. Begley, and B. N. Cox, “Generating virtual textile composite specimens using statistical data from micro-computed tomography: 3D tow representations,” *J. Mech. Phys. Solids*, vol. 60, no. 8, pp. 1561–1581, 2012.
- [18] J. Ya, Z. Liu, and Y. Wang, “Micro-CT Characterization on the Meso-Structure of Three-Dimensional Full Five-Directional Braided Composite,” *Appl. Compos. Mater.*, pp. 1–18, 2016.
- [19] P. Badel and E. Maire, “X-ray tomography analysis of the mechanical behaviour of reinforcements in composites,” *Compos. Reinf. Optim. Perform.*, pp. 565–587, 2011.
- [20] J. E. Little, X. Yuan, and M. I. Jones, “Characterisation of voids in fibre reinforced composite materials,” *NDT E Int.*, vol. 46, pp. 122–127, Mar. 2012.
- [21] F. Desplentere, S. V. Lomov, D. L. Woerdeman, I. Verpoest, M. Wevers, and a. Bogdanovich, “Micro-CT characterization of variability in 3D textile architecture,” *Compos. Sci. Technol.*, vol. 65, no. 13, pp. 1920–1930, Oct. 2005.
- [22] G. W. Melenka, E. Lepp, B. K. Cheung, and J. P. Carey, “Micro-computed tomography analysis of tubular braided composites,” *Compos. Struct.*, vol. 131, pp. 384–396, 2015.
- [23] N. Abdelal and S. L. Donaldson, “Comparison of methods for the characterization of voids in glass fiber composites,” *J. Compos. Mater.*, p. 002199831771008, 2017.
- [24] K. Xu and X. Qian, “An FEM analysis with consideration of random void defects for predicting the mechanical properties of 3d braided composites,” *Adv. Mater. Sci. Eng.*, vol. 2014, 2014.
- [25] R. C. Gonzalez, *Digital image processing*. Prentice Hall YR - 2002.
- [26] G. W. Melenka and J. P. Carey, “Development of a generalized analytical model for tubular braided-architecture composites,” *J. Compos. Mater.*, 2017.
- [27] L. Xu, C. Z. Jin, and S. Kyu Ha, “Ultimate strength prediction of braided textile composites using a multi-scale approach,” *J. Compos. Mater.*, no. January, p. 0021998314521062-, 2014.
- [28] C. S. Lee, S. G. Kim, H. J. Kim, and S. H. Ahn, “Measurement of anisotropic compressive strength of rapid prototyping parts,” *J. Mater. Process. Technol.*, vol. 187–188, pp. 627–630, 2007.